Domain Orientation in the Inactive Response Regulator *Mycobacterium tuberculosis* MtrA Provides a Barrier to Activation[†,‡]

Natalia Friedland,[§,||] Timothy R. Mack,[§,#] Minmin Yu,[○] Li-Wei Hung,[⊥] Thomas C. Terwilliger,[||] Geoffrey S. Waldo,[||] and Ann M. Stock*[,#,▽]

Bioscience Division and Physics Division, Los Alamos National Laboratory, Los Alamos, New Mexico 87545, Department of Biochemistry, Robert Wood Johnson Medical School, University of Medicine and Dentistry of New Jersey, Piscataway, New Jersey 08854, Howard Hughes Medical Institute, Chevy Chase, Maryland 20815-6789, and Physical Biosciences, Lawrence Berkeley National Laboratory, Berkeley, California 94720

Received December 12, 2006; Revised Manuscript Received March 15, 2007

ABSTRACT: The structure of MtrA, an essential gene product for the human pathogen *Mycobacterium tuberculosis*, has been solved to a resolution of 2.1 Å. MtrA is a member of the OmpR/PhoB family of response regulators and represents the fourth family member for which a structure of the protein in its inactive state has been determined. As is true for all OmpR/PhoB family members, MtrA possesses an N-terminal regulatory domain and a C-terminal winged helix-turn-helix DNA-binding domain, with phosphorylation of the regulatory domain modulating the activity of the protein. In the inactive form of MtrA, these two domains form an extensive interface that is composed of the α4-β5-α5 face of the regulatory domain and the C-terminal end of the positioning helix, the trans-activation loop, and the recognition helix of the DNA-binding domain. This domain orientation suggests a mechanism of mutual inhibition by the two domains. Activation of MtrA would require a disruption of this interface to allow the α4-β5-α5 face of the regulatory domain to form the intermolecule interactions that are associated with the active state and to allow the recognition helix to interact with DNA. Furthermore, the interface appears to stabilize the inactive conformation of MtrA, potentially reducing the rate of phosphorylation of the N-terminal domain. This combination of effects may form a switch, regulating the activity of MtrA. The domain orientation exhibited by MtrA also provides a rationale for the variation in linker length that is observed within the OmpR/PhoB family of response regulators.

Histidine protein kinases (HKs[1]) and response regulators (RRs) are the two conserved proteins found in two-component signal transduction pathways (*1*, *2*). Two-component systems (TCSs) couple environmental stimuli to cellular responses that in most cases are elicited through transcriptional regulation, resulting in alterations in gene expression. Intracellular processes that are regulated by these pathways include motility, virulence, nutrient uptake, metabolism, and quorum sensing (*3*−*6*). Output responses are controlled by the phosphorylation state of the RR, with phosphorylation of a conserved aspartate residue typically corresponding to the active state. The level of phosphorylation of the RR is regulated by the HK and by the RR itself. HKs have ATP-dependent autophosphorylation activity, generating high-energy phosphohistidines that serve as substrates for phosphotransfer to RRs. Some HKs also possess a phosphatase activity that is directed against the cognate RR. These two enzymatic activities are modulated by environmental signals that are either directly or indirectly sensed by the HK. In addition to the regulation mediated by the HK, each RR possesses a characteristic auto-dephosphorylation activity that further influences RR phosphorylation levels. Although the minimal TCS consists of a single HK and its cognate RR, many TCS pathways involve auxiliary proteins that provide additional regulatory features to the central phosphotransfer scheme.

The majority of RRs are multidomain proteins consisting of a conserved regulatory domain that contains the site of phosphorylation and a variable effector domain, the activity of which is influenced by the regulatory domain. RRs are classified into families on the basis of the sequence and structural similarity of their effector domains (*7*, *8*). Most RRs are transcription factors that are divided into subfamilies on the basis of the type of DNA-binding effector domain that they possess. The most populated subfamily, representing approximately one-third of all RRs identified to date, is the

[†] This work was supported by NIH Grants R37GM047958 (to A.M.S.), and U54 GM074946 (to T.C.T.).

[‡] The coordinates and structure factor amplitudes have been deposited with the Protein Data Bank; pdb code: 2GWR.

* To whom correspondence should be addressed. Tel: (732) 235-4844. Fax: (732) 235-5289. E-mail: stock@cabm.rutgers.edu.

[§] These two authors contributed equally to this work.

[||] Bioscience Division, Los Alamos National Laboratory.

[⊥] Physics Division, Los Alamos National Laboratory.

[#] University of Medicine and Dentistry of New Jersey.

[▽] Howard Hughes Medical Institute.

[○] Lawrence Berkeley National Laboratory.

[1] Abbreviations: BME, β-mercaptoethanol; HK, histidine kinase; HPLC, high performance liquid chromatography; HTH, helix-turn-helix; IPTG, isopropyl-1-thio-β-D-galactopyranoside; MAD, multiple-wavelength anomalous diffraction; $MtrA_N$, N-terminal regulatory domain (residues 1−125) of MtrA; ORF, open reading frame; PCR, polymerase chain reaction; PAGE, polyacrylamide gel electrophoresis; rmsd, root mean square deviation; RR, response regulator, TCS, two-component system.

10.1021/bi602546q CCC: $37.00
Published on Web 05/19/2007

OmpR/PhoB subfamily (*8*) that is characterized by a winged HTH DNA-binding domain (*9*). Phosphorylation of the regulatory domain of OmpR/PhoB family members enhances their ability to bind DNA and regulate transcription (*10*, *11*), and this is generally correlated with enhanced dimerization or higher order oligomerization (*12*−*16*). However, the molecular mechanisms that underlie phosphorylation-mediated activation are not well defined for members of the OmpR/PhoB family because there is a limited amount of information that compares the relationship between regulatory and DNA-binding domains in both inactive and active states.

It is well established that phosphorylation of a conserved Asp residue in the regulatory domain (Asp 56 in MtrA) modulates the activity of RRs. The conformational changes within the regulatory domain that are facilitated by phosphorylation have been characterized for several proteins (*17*−*20*), including an OmpR/PhoB family member (*21*). These analyses have led to a model of activation that involves two highly conserved residues, a Ser or Thr residue (Thr 83 in MtrA) that is located at the C-terminal end of β4 and a Tyr or Phe residue (Tyr 102 in MtrA) found in the middle of β5. The inactive state of the protein is associated with a conformation in which the hydroxyl group of the Ser/Thr side chain points away from the active site, and the Tyr/Phe residue extends outward from the surface of the regulatory domain. Conversely, in the active state, the hydroxyl group of the Ser/Thr residue points toward the active site, in a position where it can interact with the phosphorylated Asp residue, and the Tyr/Phe residue is buried. These two states exist in equilibrium with phosphorylation of the regulatory domain shifting the equilibrium toward the active state (*22*). The reorientation of these two residues between inward and outward conformations provides a means of coupling phosphorylation at one location of the protein to rearrangement of residues at a distal face.

Recent structural characterization of isolated regulatory domains of OmpR/PhoB family members has provided insight into the active state dimer. A single regulatory domain dimer conformation has been observed for all OmpR/PhoB family members that have been crystallized in their active states, stabilized in this form either by the presence of the phosphoryl analogue beryllofluoride or by the high protein concentrations used in crystallization (*21*, *23*−*25*). The α4-β5-α5 faces of the domains are juxtaposed, forming a rotationally symmetric dimer. The interface consists of a small hydrophobic patch and an extensive network of salt bridges involving residues that are highly and exclusively conserved within the regulatory domains of OmpR/PhoB family members, lending support to the notion that all OmpR/PhoB transcription factors adopt a common active state (*21*, *24*, *25*). Flexible linkers are presumed to connect the regulatory domains to the DNA-binding domains that associate with head-to-tail symmetry to bind to the direct repeat DNA half-sites that comprise most binding sites for OmpR/PhoB transcription factors (*26*−*30*).

Substantially greater structural diversity exists in the inactive states of OmpR/PhoB transcription factors. To date, three structures of inactive full-length OmpR/PhoB transcription factors have been reported (*16*, *31*, *32*) along with the structures of isolated inactive regulatory domains of two OmpR/PhoB family members that form alternative dimers, distinct from the α4-β5-α5 active state dimer (*21*, *33*, *34*). These structures all display distinctly different intra and intermolecular domain interactions.

Here, we report the crystal structure of inactive MtrA, an OmpR/PhoB family member from *Mycobaterium tuberculosis*, a major human pathogen that currently infects nearly 2 billion people worldwide. MtrA is an essential protein in *M. tuberculosis* (*35*, *36*) and is differentially expressed in virulent and avirulent strains during growth in macrophages (*36*), making it a potential antimicrobial drug target. The structure of MtrA provides a foundation for understanding the regulation of its activity within the MtrB/MtrA TCS pathway. It expands the repertoire of structures of inactive full-length OmpR/PhoB transcription factors and provides a rationale for the variation in inter-domain linker lengths in OmpR/PhoB family members. Our data support the hypothesis that diverse inactive states among OmpR/PhoB RRs provide different strategies of regulation that can be adapted to the specific needs of each individual TCS.

MATERIALS AND METHODS

Materials. Unlabeled ammonium hydrogen phosphoramidate was synthesized by the method of Sheridan et al. (*37*). [^{32}P]ammonium hydrogen phosphoramidate was synthesized according to a modified version of the method developed by Buckler and Stock (*38*). In order to increase the specific activity of the phosphoramidate, the quantities of all reagents except [^{32}P]orthophosphoric acid were reduced 2-fold but were maintained at the same molar concentrations as previously described. This modification resulted in about half the yield with a 2-fold increase in the specific activity.

Protein Production and Purification. His-Tagged MtrA. DNA encoding the *M. tuberculosis mtrA* gene was amplified by PCR from *M. tuberculosis* H37Rv genomic DNA (obtained from Mycobacteria Research Laboratories (MRL) at Colorado State University) and cloned into a pET28a-based expression vector (*39*) using the *Nde*I and *Spe*I restriction sites. The resulting vector, which encoded residues 1−228 of MtrA, as annotated in *M. tuberculosis* genome databases (sequence tag Rv3246c; http://genolist.pasteur.fr/TubercuList/ and http://www.doe-mbi.ucla.edu/TB/PUBLIC/qs/qsearch_proteomic.php?orf=Rv3246c; GenBank: CAB08347), and the additional amino acids TSGSHHHHHH on the C-terminus of MtrA, was transformed into BL21-Gold (DE3) *Escherichia coli* cells (Stratagene). The translational start site of *mtrA* identified by the *M. tuberculosis* genome sequencing project and used in this study is 3 codons upstream of that indicated in other database entries (GenBank: AAB07804; UniProt: P0A5Z4; Swiss-Prot: Q50447). In order to obtain selenomethionine-substituted protein, the cells were grown in M9 minimal media supplemented with 0.2% glucose, 2 mM $MgSO_4$, 1 μM $CaCl_2$, 0.005% thiamine, 35 mg/mL kanamycin, and 0.02 mg/mL Ala, Asp, Lys, Arg, His, Pro, Gly, Thr, Ser, Gln, Asn, Ile, Phe, and Trp; 100 mg/mL Thr, Lys, and Phe; 50 mg/mL Leu, Ile, and Val, and 60 mg/mL L-selenomethionine. Cells were grown at 37 °C to mid-log phase, and expression was induced by the addition of IPTG to a final concentration of 0.5 mM. After a 4 h incubation period at 37 °C, the cells were harvested by centrifugation. Cell pellets were resuspended in a buffer containing 20 mM Tris-HCl at pH 8.0 and 150 mM NaCl (buffer A), and lysed

by sonication. The cell lysate was clarified by centrifugation (30,000*g*) for 40 min. The soluble fraction of the lysate was incubated for 1 h at 4 °C with 1.5 mL of Talon resin (Clontech), pre-equilibrated with buffer A, per 1.5 L of cell culture. The resin was washed once with 15 mL of buffer A, transferred to a gravity-flow column (Bio-Rad), washed with an additional 15 mL of buffer A, and eluted with 250 mM imidazole in buffer A. The resulting sample was loaded onto a Superdex 75 26/60 gel filtration column (General Electric) that was pre-equilibrated with 10 mM Tris at pH 8.0, 100 mM NaCl, and 10 mM BME buffer. The fractions containing MtrA were pooled and concentrated.

Native MtrA. For the expression of native MtrA, *E. coli* BL-21(DE3) cells carrying a plasmid encoding *mtrA* were grown at 37 °C in Luria−Bertani media containing 100 μg/mL kanamycin to mid-log phase and then transferred to 20 °C. Expression of MtrA was induced by the addition of IPTG to a final concentration of 0.5 mM, and growth was continued for 14 h. The cells were harvested by centrifugation and lysed by sonication in buffer A. The lysate was clarified by centrifugation (50,000*g*) for 1 h. The soluble portion of MtrA was precipitated by the addition of ammonium sulfate to a final concentration of 50% w/v. The ammonium sulfate pellet was resuspended in 20 mM Tris at pH 8.0 and then dialyzed extensively against the same buffer. The extract was then applied to a 5-mL HiTrapQ anion exchange column (General Electric) pre-equilibrated with 20 mM Tris at pH 8.0 and eluted using a linear gradient of 20 mM Tris at pH 8.0 and 2 M NaCl. The fractions containing MtrA were then applied to a Superdex 75 26/60 gel filtration column pre-equilibrated in 10 mM Tris at pH 8.0, 100 mM NaCl, and 10 mM BME. The resulting fractions containing purified MtrA were pooled and concentrated.

Native $MtrA_N$. The nucleotide sequence encoding residues 1−125 of MtrA (numbering scheme as described above) was amplified using a plasmid containing the full-length sequence of *mtrA* as a template. The PCR product was cloned into pJES307 using the unique restrictions sites *Nde*I and *Hin*dIII and then transformed into *E. coli* BL21(DE3) cells. Cells were grown at 37 °C in Luria−Bertani media containing 100 μg/mL amplicillin to mid-log phase and then transferred to 20 °C before expression of $MtrA_N$ was induced by the addition of IPTG to a final concentration of 0.5 mM. After growing the cells for an additional 15 h at 20 °C they were harvested by centrifugation and lysed by sonication in 100 mM sodium phosphate at pH 7.0. After the lysate was clarified by ultracentrifugation (80,000*g*) the soluble portion of $MtrA_N$ was precipitated by the addition of ammonium sulfate to a final concentration of 40% w/v. The ammonium sulfate pellet was resuspended in 20 mM Bis-Tris at pH 7.5 and then dialyzed extensively against the same buffer. The protein was then applied to a 5-mL HiTrapQ anion exchange column pre-equilibrated with 20 mM Bis-Tris at pH 6.75 and eluted using a linear gradient of 20 mM Bis-Tris at pH 6.75 and 1 M NaCl. Fractions containing MtrA were then applied to a Superdex 75 26/60 gel filtration column pre-equilibrated with 10 mM Tris at pH 6.75, 100 mM NaCl, and 10 mM $MgCl_2$.

Protein Crystallization and Data Collection. His_6-tagged MtrA was concentrated to 5 mg/mL in 10 mM Tris at pH 8.0, 100 mM NaCl, and 10 mM BME, and 100 × 20 × 20 μm^3 crystals formed spontaneously after one week of storage at 4 °C. These were cryoprotected using 25% glycerol and frozen in liquid nitrogen. The crystals, which diffracted to 2.5 Å, belonged to space group $P2_12_12_1$. The dimensions of the unit cell were: $a = 38.9$ Å, $b = 56.6$ Å, and $c = 135.1$ Å with one molecule per asymmetric unit. Multiwavelength dispersion data were collected from a single crystal at ALS beamline 8.2.1. A 2.1 Å dataset was collected at ALS beamline 5.0.2. The data were processed with DENZO and scaled with SCALEPACK (*40*).

Structure Determination and Refinement. Phases were determined by MAD using the program autoSHARP (*41*) and the resulting electron density map was used to automatically build ∼90% of the structure with the program ARP/wARP (*42*). The model was completed using the program Coot (*43*). The structure was refined using a dataset from a different selenomethionine-substituted crystal as a native dataset because it diffracted to a higher resolution. Refinement of the structure was carried out using the program PHENIX (*44*) with rebuilding of the model between refinement cycles in Coot. No density was observed for the C-terminal His-tag. The final model consists of residues 2−228 of MtrA with the exception of residues 187−188 and the side chains of Asp 2, Arg 122, and Arg 170 for which no electron density was observed. The numbering scheme used for the model of MtrA is based on the annotation in the *M. tuberculosis* genome database; thus, residues 2−228 in the structural model of MtrA correspond to residues 1−225 in previous studies (*35*, *36*, *45*). In addition, 92 water molecules, 2 glycerol molecules, and a Ca^{2+} bound at the active site were also identified. The crystallographic *R*-factor is 20.4%, and R_{free} is 24.4%. All residues fall in the allowed region of the Ramachandran plot. Data collection and refinement statistics are shown in Table 1. The superpositions and rmsd calculations were done using the programs Coot and ProFit (Martin, A. C. R., http://www.bioinf.org.uk/software/profit/) and the Figures were generated using MolScript (*46*) and Raster3D (*47*).

MtrA and $MtrA_N$ Phosphorylation Assays. Phosphorylation was performed by incubating 12 μM MtrA or $MtrA_N$ or 2.4 μM $MtrA_N$ in a reaction mixture containing 50 mM ammonium hydrogen phosphoramidate, 10 mM Tris-HCl at pH 7.8, 100 mM NaCl, 10 mM $MgCl_2$, and 2 mM BME. Proteins were incubated at room temperature, and aliquots were removed at indicated intervals. Either 62 μg of MtrA or 28 μg of $MtrA_N$, each in a volume of 200 μL, was injected onto a C-8 reverse-phase HPLC column (Grace-Vydac Cat# 208TP5415) pre-equilibrated in 31.5% actetonitrile and 0.1% trifluoroacetic acid. Proteins were eluted using a 20-mL gradient from 31.5% acetonitrile and 0.1% trifluoroacetic acid to 58.5% acetonitrile and 0.1% trifluoroacetic acid at a flow rate of 1 mL/min. Analytical gel filtration was performed using a Superdex S75 10/300 GL column (General Electric Cat# 17-5174-01) at a flow rate of 0.7 mL/min. MtrA or $MtrA_N$, 12 μM or 10 μM, respectively, in a volume of 200 μL were loaded onto the column pre-equilibrated with 10 mM Tris-HCl at pH 7.8, 100 mM NaCl, and 2 mM BME.

Phosphorylation of MtrA and $MtrA_N$ with [^{32}P]Phosphoramidate. MtrA or $MtrA_N$ at a final concentration of 15 μM was incubated in the presence of 20 mM [^{32}P]phosphoramidate (specific activity = 70.1 CPM/pmol), 10 mM $MgCl_2$, 50 mM Tris-HCl at pH 7.5, 100 mM NaCl, and 2 mM BME in a 60-μL reaction mixture. The reaction was quenched by

Table 1: Data Collection and Refinement Statistics

			MAD	
	high resolution	$\lambda_{inflection}$	λ_{peak}	λ_{remote}
		data collection		
space group	$P2_12_12_1$			
unit cell parameters: *a*, *b*, *c* (Å)	38.9, 56.6, 135.1			
resolution limits (Å)	50−2.1 (2.18−2.10)[a]	50−2.6 (2.69−2.60)	50−2.5 (2.59−2.50)	50−2.7 (2.80−2.70)
wavelength (Å)	0.9793	0.9797	0.9796	0.9184
no. of reflections: total/unique	18121/1970	6531/759	10591/1375	5609/630
R_{sym}[b] (%)	10.4 (26.0)	11.1 (47.2)	11.0 (42.0)	11.1 (41.8)
		refinement		
resolution limits (Å)	43−2.1			
R_{cryst}[c]/R_{free}[d] (%)	20.4/24.4			
no. of protein atoms	1746			
no. of water atoms	92			
rmsd bond lengths (Å)	0.01			
rmsd bond angles (°)	1.6			
average *B* factor (Å^2)	33.9			

[a] The numbers in parentheses refer to the highest resolution shells. [b] $R_{sym} = \Sigma|I_{obs} - I_{avg}|/\Sigma I_{avg}$. [c] $R_{cryst} = \Sigma|F_o(hkl) - F_c(hkl)|/\Sigma|F_o(hkl)|$. [d] $R_{free} = R_{cryst}$, calculated for 5% of randomly selected reflections that are not included in the refinement.

mixing 5 μL of the reaction mixture, which corresponds to 75 pmol of protein, with 2 μL of quench solution containing 1.25% sodium dodecyl sulfate and 50 mM EDTA. The entire 7 μL of the quenched reaction was immediately spotted onto 0.8-cm squares of nitrocellulose membrane and washed three times in a chilled buffer containing 50 mM Tris-HCl at pH 7.5, 100 mM NaCl, and 2 mM BME. Nitrocellulose squares were immersed in 2 mL of Ecoscint A (National Diagnostics), and radioactivity was measured using a Beckman LS 6500 scintillation counter.

RESULTS

Overall Structure. The structure of MtrA was determined and refined at 2.1 Å resolution as described in Materials and Methods. As is true for other members of the OmpR/PhoB family, MtrA contains two domains, an N-terminal regulatory domain exhibiting the classic α/β fold observed in all RRs and a C-terminal effector domain with a winged HTH DNA-binding fold (Figure 1). In MtrA, the two domains are connected to each other by a flexible linker and form an extensive interface. A comparison of MtrA with the three other OmpR/PhoB proteins for which full-length structures have been determined (*16*, *31*, *32*) shows that the most significant differences between them lie not in the conformations of the individual domains but in how the domains are oriented relative to each other. The domain orientation and inter-domain interface exhibited by MtrA are most similar to, yet distinct from, those found in *M. tuberculosis* PrrA (*32*).

Inactive Conformation of MtrA. Unphosphorylated His_6-tagged MtrA was crystallized in the absence of any phosphoryl analogues and was therefore expected to exist in an inactive state. In the experimental maps, the active site region of MtrA contained strong electron density indicative of a metal ion, although no divalent cations were included during crystallization. The ion is coordinated to six ligands: three water molecules, the side chain oxygens of Asp 56 and Asp 13, and the backbone carbonyl oxygen of Met 58 (Figure 2), identical to the ligands that bind Mg^{2+} or Ca^{2+}

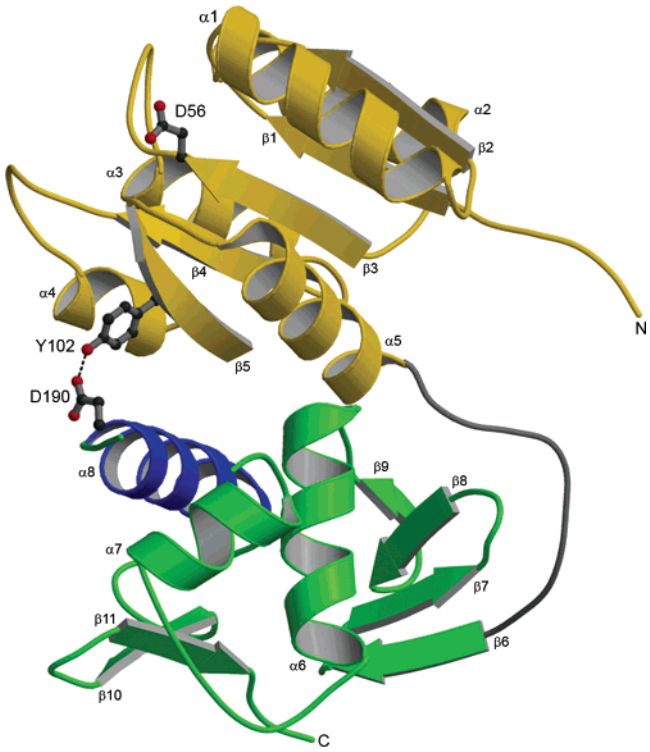

FIGURE 1: Ribbon depiction of MtrA. The regulatory domain is shown in gold, and the DNA-binding domain is shown in green with the recognition helix, α8, highlighted in blue. The side chains of Asp 56, the site of phosphorylation, and Tyr 102 and Asp 190 that form an inter-domain hydrogen bond are shown in ball-and-stick format with the hydrogen bond depicted by a dashed line.

in other RR structures (*32*, *48*). However, the geometry is significantly distorted from the octahedral coordination expected for Mg^{2+}, and the relatively long 2.33−2.73 Å protein−metal ion bond lengths observed in the MtrA structure are a better match to those expected for Ca^{2+} than for Mg^{2+} (*49*). The electron density has been modeled as a Ca^{2+}, but the true identity of this ligand remains uncertain. As anticipated for the inactive regulatory domain, the side chain of Thr 83 is oriented away from the active site, and

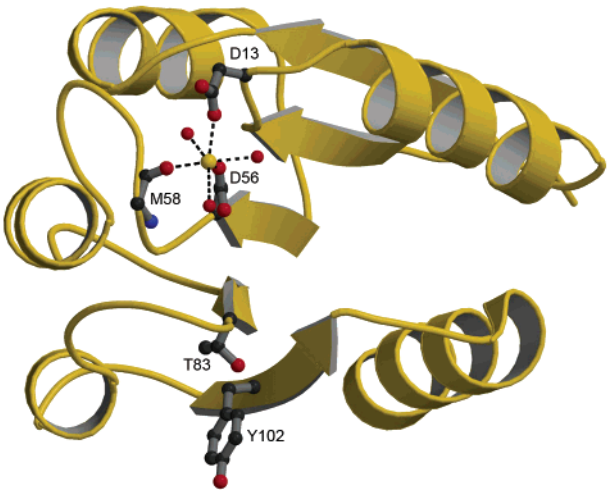

FIGURE 2: Active site and switch residues in the regulatory domain of MtrA. The metal ion, modeled as Ca^{2+} (yellow sphere), is coordinated by the side chains of Asp 13 and Asp 56, the backbone carbonyl oxygen of Met 58 (ball-and-stick representation), and three water molecules (red spheres). The side chains of the two conserved switch residues that display distinctly different orientations in inactive and active regulatory domains, Thr 83 and Tyr 102, are shown (ball-and-stick representation).

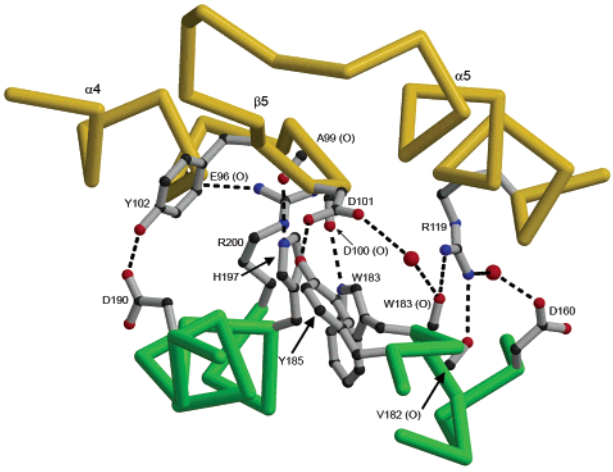

FIGURE 3: Inter-domain interface in inactive MtrA. A Cα trace of juxtaposed regions of the regulatory (gold) and DNA-binding domain (green), with the recognition helix in blue, are shown along with the side chains and several backbone carbonyls of residues that contribute to the domain interface (ball-and-stick representation). Water molecules are shown as red spheres and hydrogen bonds as dashed lines.

Tyr 102 is in an outward position (Figure 2). Tyr 102 forms a hydrogen bond with Asp 190 of the DNA-binding domain (Figure 1). These features support the conclusion that this crystal structure represents the inactive state of MtrA. In the active state, Tyr 102 would be expected to adopt an inward orientation, necessitating the disruption of the Tyr 102−Asp 190 hydrogen bond and a weakening of the domain interface. It is interesting to note that in the crystal structures of *Thermotoga maritima* DrrB (*16*) and *M. tuberculosis* PrrA (*32*), which also represent inactive states with extensive domain interfaces, the analogous Tyr residue forms a hydrogen bond with the DNA-binding domain, but in each of the three proteins, the contact involves a different residue within the DNA-binding domain.

Inter-Domain Interface of MtrA. The inter-domain interface of MtrA buries approximately 800 Å^2 of each domain and consists of the α4-β5-α5 face of the regulatory domain and the C-terminal end of α7, the α7-α8 loop, and α8 of the DNA-binding domain. Both faces that contribute to this interface have been shown in other OmpR/PhoB family members to form functionally important protein−protein or protein−nucleic acid interactions in the active state. The α4-β5-α5 face of the regulatory domain of OmpR/PhoB RRs is used for the formation of a symmetric dimer in the active state (*21*, *23*−*25*), and it is well established that the recognition helix (α8) and possibly also the transactivation loop (α7-α8 loop) are required for interaction with DNA and RNA polymerase, respectively (*9*, *30*, *50*).

The residues from the regulatory domain that comprise the interface are contributed primarily from α4, the N-terminal half of β5, and the extreme C-terminal end of α5 (Figure 3). This subset of residues covers approximately half of the total area of the α4-β5-α5 face with the boundary between the residues that contribute to the interface and those that do not forming a diagonal that traverses this face from the N-terminal end of α4 to the C-terminal end of β5. Both hydrophobic and polar interactions stabilize the interface. However, there is no central hydrophobic patch in the domain interface of MtrA or PrrA (*32*), unlike the interface observed in DrrB (*16*). From the regulatory domain, Val 92, Leu 95, and Tyr 102 contribute to the hydrophobic portion of the interface contacting Trp 183, Leu 193, Val 196, and Leu 157 in the DNA-binding domain. In addition to the hydrophobic interactions, there are a total of 9 hydrogen bonds, including the aforementioned hydrogen bond between Tyr 102 and Asp 190. Thus, the domain interface involves residues that are central to the activation of the regulatory domain, specifically, Tyr 102, the aromatic residue involved in the conserved switch mechanism, and Val 92, Leu 95, Glu 96, and Asp 101, hydrophobic and charged residues that form the conserved active state dimer interface of OmpR/PhoB RRs (*21*, *24*).

Linker Region. The C terminus of the regulatory domain of MtrA lies in close proximity to the inter-domain interface, whereas the N terminus of the DNA-binding domain is distally positioned (Figure 1). The linker that connects the two domains must therefore traverse almost half the circumference of the DNA-binding domain. The linker of MtrA is about nine residues in length and adopts an extended conformation that appears to be relatively flexible. The average *B*-factor for all backbone atoms of MtrA is 30.6 Å^2, whereas within the linker region, some residues have *B*-factors greater than 50 Å^2. The linker is not tightly packed against the DNA-binding domain, and only one contact is observed, a hydrogen bond between Glu 126 and His 143. Thus, the linker functions to tether the two domains without significantly contributing to the packing forces that stabilize their interaction in the inactive state.

Comparison to Other Full-length OmpR/PhoB Family Members. Of the three other full-length OmpR/PhoB family members for which crystal structures have been determined, the domain orientation exhibited by MtrA is most similar to that exhibited by PrrA (*32*) (Figure 4). In both crystal structures, the α4-β5-α5 face of the regulatory domain is packed against the face of the DNA-binding domain that is formed by the positioning helix (α7), the transactivation loop (α7-α8) and the recognition helix (α8). This orientation is

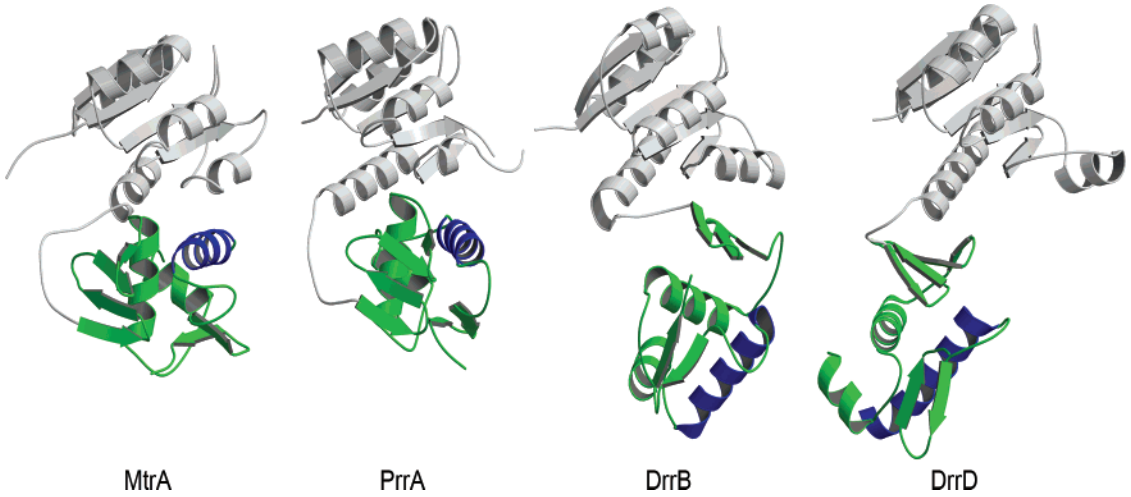

FIGURE 4: Domain orientations in *M. tuberculosis* MtrA, *M. tuberculosis* PrrA, *T. maritima* DrrB, and *T. maritima* DrrD (pdb codes: 1YS6, 1P2F, and 1KGS). Ribbon diagrams of the four structurally characterized inactive OmpR/PhoB family RRs (*16*, *31*, *32*) are shown in orientations obtained by superimposition of their regulatory domains (gray). The effector domains (green) and recognition helices (blue) have different relative orientations in each protein.

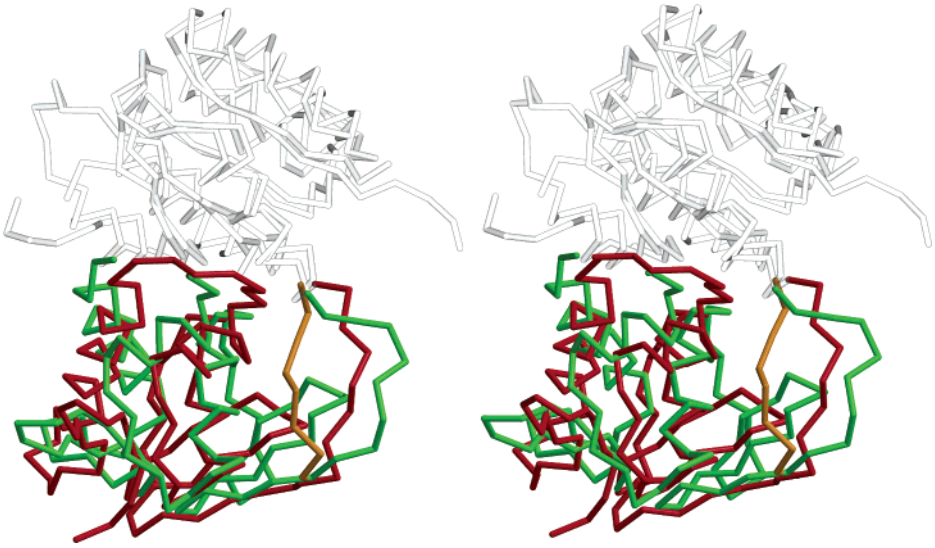

FIGURE 5: Stereoview of superimpositions of *M. tubercuolisis* MtrA and PrrA. MtrA and PrrA (molecules A and B) were aligned by superimposition of their regulatory domains using ProFit. Cα traces of MtrA (regulatory domain gray, linker and DNA-binding domain green), PrrA molecule A (regulatory domain gray, linker and DNA-binding domain red) are shown, and for clarity, only the linker region of PrrA molecule B (gold) is shown.

significantly different from that observed for both *T. maritima* DrrB and DrrD in which the β-platform of the DNA-binding domain is juxtaposed to the α4-β5-α5 face of the regulatory domain (*16*, *31*). In DrrB these faces form an extensive interface. DrrD lacks a defined interface, but the short linker constrains these same two faces to close proximity.

Although MtrA and PrrA appear to be similar to each other in overall structure with rmsds of 1.9 and 2.0 Å for backbone atoms of the regulatory and effector domains, respectively, superimposition of the two proteins reveals subtle differences in both the domain orientations and the conformations of the linkers (Figure 5). Specifically, when the regulatory domains of PrrA and MtrA are superimposed, the DNA-binding domains are misaligned (rmsd for backbone atoms, 9.9 Å) because of a small rotation around an axis roughly perpendicular to the plane of the domain interface. Many of the same inter-domain interactions present in the interface of MtrA also occur in PrrA. However, there are several interactions that are not conserved. The most notable of these is the hydrogen bond formed between the conserved aromatic residue in the regulatory domain and its bonding partner in the DNA-binding domain. In MtrA, this hydrogen bond involves Tyr 102 and Asp 190, whereas in PrrA, Tyr 105 forms a bond with Asn 198 rather than with Asp 196, the residue corresponding to Asp190 in MtrA. Not surprisingly, in DrrB, which has a significantly different orientation of the DNA-binding domain, the analogous Tyr residue (Tyr 97) forms a hydrogen bond with yet a different residue, Asp 131. Although the three structures display different inter-domain interfaces and distinct hydrogen bond partners for the conserved aromatic switch residue, the presence of a Tyr-Asp/Asn bond that bridges the domains appears to provide a common element in the coupling of phosphorylation to destabilization of the domain interface.

In both MtrA and PrrA there is evidence of flexibility in the linker, suggesting that it may adopt multiple conformations. PrrA crystallized in the *P*1 space group with two

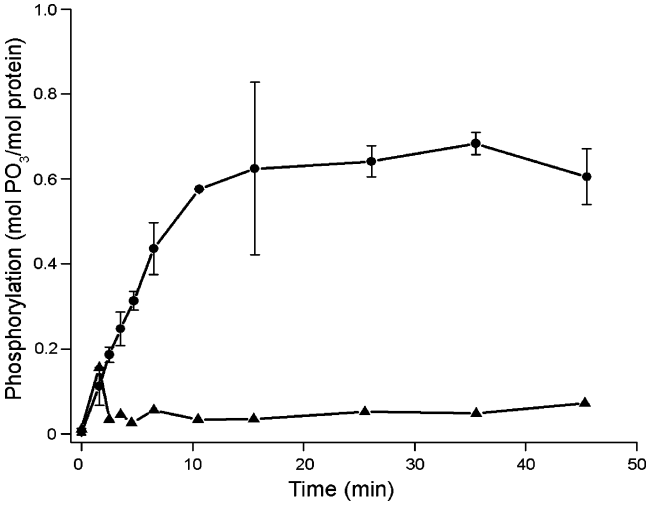

FIGURE 6: Phosphorylation of $MtrA_N$ and MtrA with [^{32}P]labeled phosphoramidate. Phosphorylation of $MtrA_N$ (●) and MtrA (▲) was carried out as described in Materials and Methods. The error bars for $MtrA_N$ represent one standard deviation between two replicates.

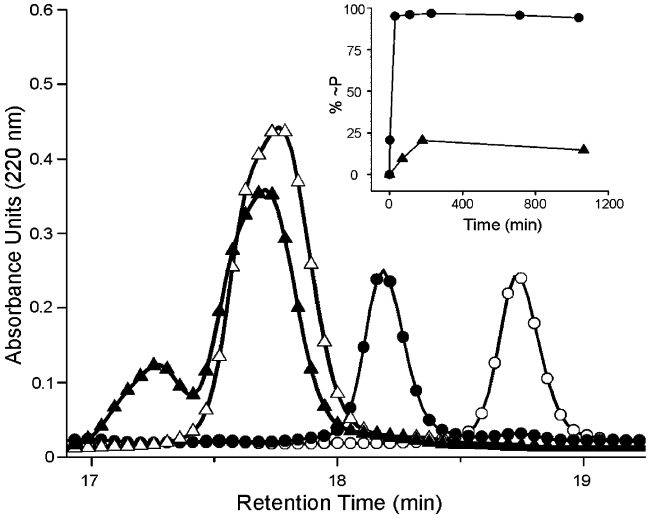

FIGURE 7: HPLC analysis of MtrA and $MtrA_N$ phosphorylation. MtrA (▲, △) and $MtrA_N$ (●, ○) incubated in the absence (△, ○) or presence (▲, ●) of phosphoramidate were analyzed by reverse-phase HPLC as described in Materials and Methods. HPLC profiles shown for the phosphoramidate-treated proteins correspond to steady-state levels obtained at 30 min for $MtrA_N$ and 180 min for MtrA. The time courses of phosphorylation for MtrA (▲) and $MtrA_N$ (●) are shown in the inset. For each point, the percentage of protein phosphorylated (% ~P) was calculated from the integrated area of the fastest migrating species divided by the total integrated area of both peaks.

molecules in the asymmetric unit (A and B) (*32*). The linker region is significantly different in the two molecules. In PrrA molecule A, the C terminus of helix α5 continues for one additional turn, and the linker that extends from it is positioned away from the DNA-binding domain. In the other molecule, with a shorter α5, the linker packs closely, though imperfectly, against the DNA-binding domain. Inspection of the lattice contacts experienced by the two molecules of PrrA suggests that crystal-packing forces influence the conformations of the linker regions. The linker in MtrA, which has little contact with the DNA-binding domain, is most similar to the linker in molecule A of PrrA, and it too contacts other molecules in the crystal lattice. The different conformations of the linkers, their minimal contacts with the DNA-binding domains, and their relatively high *B*-factors all indicate inherent flexibility in the linkers of these two RRs.

Solution Studies of MtrA and $MtrA_N$. Many RRs have an increased propensity for dimerization or higher order oligomerization upon phosphorylation (*12*−*16*). The oligomeric states of MtrA and the isolated regulatory domain, $MtrA_N$ (residues 1−125), were assessed in the absence and presence of small molecule phosphodonors (*51*). Purified proteins were incubated with phosphoramidate and phosphorylation was assessed by either measuring incorporation of [^{32}P]phosphoryl groups or, using unlabeled phosphoramidate, by reverse-phase HPLC under conditions in which phosphorylated and unphosphorylated RRs can typically be distinguished by different chromatographic mobilities. Phosphoramidate was used as the phosphodonor because of the slow rate of phosphorylation by acetyl phosphate (data not shown).

Incorporation of [^{32}P]phosphoryl groups into $MtrA_N$ occurred rapidly in the presence of 20 mM phosphoramidate, reaching a steady-state level of ~65% within 30 min, whereas no detectable phosphorylation of MtrA was observed within the same time period (Figure 6). In agreement with the [^{32}P]phosphoramidate assay, HPLC analysis of $MtrA_N$ showed complete phosphorylation within 30 min when the phosphorylation reaction was carried out with 10 μM $MtrA_N$ (Figure 7) and 50 min when the reaction contained 2.4 μM $MtrA_N$ (data not shown). The slight differences in the stoichiometry of $MtrA_N$ phosphorylation obtained in the radioactive and HPLC assays are likely a reflection of inaccuracies in estimating either the specific activity of [^{32}P]-phosphoramidate or the concentration of $MtrA_N$, or a result of the different concentrations of phosphoramidate used in the two assays, which would have impacted the steady-state levels by altering the rates of phosphorylation without affecting dephosphorylation rates. HPLC analysis of MtrA carried out over a longer time frame than the [^{32}P]phosphoramidate assay indicates that MtrA does autophosphorylate (Figure 7). However, it occurs much more slowly than that of $MtrA_N$ reaching a steady-state level of only 20% after 180 min (Figure 7 inset), a rate consistent with the lack of detection in the radioactive assay. These kinetics indicate that the inefficient phosphorylation of MtrA is due to a decreased rate of phosphorylation rather than an increased rate of dephosphoryaltion, relative to the activities of $MtrA_N$.

Similar results were obtained with proteins dialyzed against EDTA prior to the addition of excess Mg^{2+} (data not shown), suggesting that differences in divalent cations that might have co-purified with the proteins were not responsible for the different rates of phosphorylation. It should be noted that untagged proteins were used for these analyses. When His_6-tagged MtrA was incubated with phosphoramidate, a slow increase in phosphorylation that failed to reach a steady-state after 17 h was observed (data not shown), presumably due to nonspecific phosphorylation of His residues as has been described previously (*38*).

$MtrA_N$ and MtrA, incubated in the presence or absence of phosphoramidate, were analyzed by size exclusion chromatography to determine if the hydrodynamic radii of the proteins increased as a function of phosphorylation. Phosphorylated $MtrA_N$ eluted earlier than unphosphorylated $MtrA_N$, with apparent molecular masses of 27 and 20 kDa, respectively, indicative of a monomer to dimer transition of the 14 kDa regulatory domain (Figure 8). MtrA eluted with

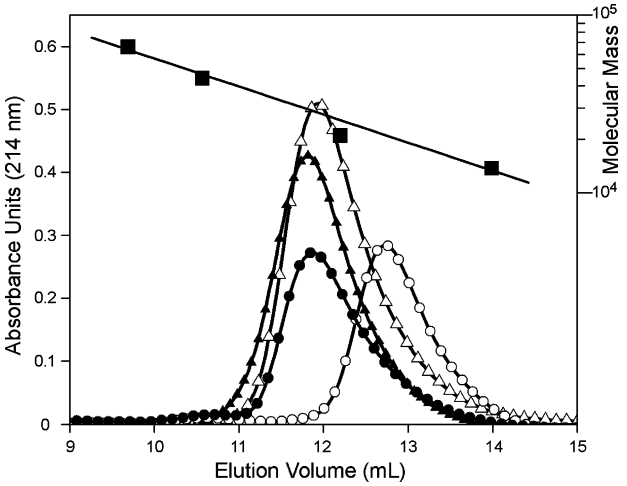

FIGURE 8: Analytical gel-filtration analysis of $MtrA_N$ and MtrA. Untreated $MtrA_N$ (○) and MtrA (△), and phosphoramidate-treated $MtrA_N$ (●) and MtrA (▲) were analyzed by analytical gel-filtration as described in Materials and Methods. The points on the standard curve correspond to bovine serum albumin (66 kDa), chicken egg albumin (44 kDa), soybean trypsin inhibitor (21 kDa), and bovine pancreas RNaseA (14 kDa).

an apparent molecular mass of 27 kDa, in agreement with its existence as a 25 kDa monomer. Incubation with phosphoramidate did not significantly alter the mobility of MtrA (Figure 8), consistent with the low level of phosphorylation detected by HPLC analysis.

DISCUSSION

Inter-Domain Interface of MtrA Suggests a Mechanism of Mutual Inhibition. RRs exist in a conformational equilibrium between inactive and active states. Phosphorylation of the regulatory domain shifts this equilibrium toward the active state. Within the OmpR/PhoB family, this is associated with increased oligomerization, enhanced DNA binding, and an increased influence on transcription. Recent structural data suggest that all OmpR/PhoB RRs adopt a common domain arrangement in the active state, in which the regulatory domains dimerize with 2-fold rotational symmetry while the effector domains align in tandem (*21*, *24*, *25*, *30*). This orientation of the DNA-binding domains is required to promote interactions with the direct repeat sequences that comprise the binding sites for OmpR/PhoB family transcription factors. The different intermolecular symmetries of the regulatory and effector domain dimers exclude the possibility of a unique intramolecular domain interface in the two protomers of the active dimer. Thus, a complete elimination of the intramolecular domain interface with a flexible linker connecting the two domains is the most likely configuration of the active state (*21*, *24*, *25*).

The structure of the OmpR/PhoB family member MtrA, described here, represents the inactive conformation of the molecule. There is no phosphoryl group or analogue in the active site, and the conformation of the two residues that have been shown to undergo a conserved repositioning upon phosphorylation (Thr 83 and Tyr 102 in MtrA) are in orientations that are associated with the inactive state. In inactive MtrA, the two domains form an extensive interface that sequesters surfaces of each domain that are functionally important to the active state: the α4-β5-α5 face of the regulatory domain and the transactivation loop (α7-α8 loop) and the recognition helix (α8) of the DNA-binding domain. In the active state, the α4-β5-α5 face is proposed to mediate dimerization of the regulatory domains, and the recognition helix and transactivation loop are important for interactions with DNA and RNA polymerase, respectively. A significant reorientation of the two domains would be required to accommodate these intermoleculecular interactions that are associated with the active state. Thus, the domain orientation and the intramolecular interface observed in inactive MtrA appear to inhibit activation through mutual inhibition of these two domains. Loss of the Tyr 102−Asp190 hydrogen bond upon reorientation of the regulatory domain switch residue, Tyr 102, and the propagated conformational change at the α4-β5-α5 face associated with phosphorylation presumably contribute to the destablization of the intramolecular domain interface that is necessary for achieving the active state.

Differences in Phosphorylation of $MtrA_N$ and MtrA. The low phosphotransfer activity of MtrA led us to examine the phosphotransfer activity of the isolated regulatory domain, $MtrA_N$, which surprisingly exhibited robust phosphorylation. There are two possible explanations for why $MtrA_N$ phosphorylated readily and MtrA did not. The less interesting of the two possibilities is that a majority of the MtrA protein is denatured and inactive, resulting in a substantially lower effective concentration. A lower concentration of native MtrA would account for both the slower rate and lower steady-state level of phosphorylation observed (20%). Though plausible, this seems unlikely for several reasons. First, we tested whether 20% active MtrA could account for this observation by examining the phosphorylation of $MtrA_N$ at 20% of the concentration that was used for MtrA. With 2.4 μM $MtrA_N$, a steady-state level of phosphorylation was attained within 50 min compared to the 180 min required for steady-state phosphorylation of MtrA. Thus, the lower rates and stoichiometries cannot be accounted for solely by a decreased population of native MtrA. In addition, MtrA is well behaved during and after purification. During both anion exchange and gel-filtration chromatography, MtrA eluted as a single species. Furthermore, the apparent molecular weight of MtrA on the basis of its elution volume from the gel-filtration column is consistent with a monomer, and the protein does not readily precipitate during storage. Additional evidence that the majority of MtrA is not misfolded is that a biologically relevant form readily crystallized, although we cannot rule out the selective crystallization of a properly folded subpopulation. If the majority of MtrA is properly folded and functional, then it must be presumed that the DNA-binding domain inhibits the phosphotransfer activity of the regulatory domain. The inhibition is substantial, producing phosphotransfer rates below the limit of detection in phosphorylation assays using [^{32}P]phosphoramidate and producing substoichiometric levels of steady-state phosphorylation, reflective of the balance between the low phosphotransfer rate and the intrinsic autodephosphorylation rate.

Inhibition of phosphotransfer activity by the DNA-binding domain is an especially interesting concept in light of emerging work in the area of protein dynamics. Conformational dynamics are an important aspect of protein function, and recent NMR studies have provided evidence that catalysis occurs specifically within a subset of the population of protein molecules that pre-exist in a catalytically competent conformation. Specifically, it has been shown that

prolyl cis−trans isomerase, CypA, samples conformations that are associated with a catalytic event in the absence of substrate and that the time scale over which these conformational changes occur corresponds to the turnover rate of the enzyme (*52*). Extrapolating this principle to RRs, which catalyze their own phosphorylation, it is possible that phosphorylation occurs exclusively in the subset of regulatory domains that exist in an active conformation.

Intra or intermolecular interactions of regulatory domains that bias the conformational equilibrium between inactive and active states might influence the propensity for phosphorylation. Our data suggest that contacts between the N- and C-terminal domains of MtrA essentially lock the regulatory domain in an inactive conformation, lowering its rate of phosphorylation. Similar inhibition of regulatory domain phosphorylation by an effector domain has been reported for FixJ (*53*). The degree of inhibition would be expected to correlate with the presence and strength of regulatory domain interactions with effector domains. Proteins such as CheY and DrrD, which lack domain interfaces and thus have the freedom to explore active states, and MtrA, with an apparently stable interface that restricts conformational freedom, represent the extremes of the spectrum. Conformational biases can be activating as well as inhibitory. Intermolecular interactions that stabilize the active states of RRs, such as the binding of peptides of CheZ and FliM to CheY and the binding of target DNA to OmpR, have been shown to increase rates of RR phosphorylation by small molecule phosphodonors (*54*, *55*).

We suggest that the intramolecular domain interface in MtrA stabilizes the inactive conformation of the regulatory domain, and inter-domain contacts involving the α4-β5-α5 face and the hydrogen bond between Tyr 102 and Asp 190 that maintains Tyr 102 in an outward orientation trap the regulatory domain in the inactive conformation. It is possible that by shifting the conformational equilibrium toward the inactive state a smaller population of molecules is competent for phosphorylation, thus explaining the decreased rate of phosphorylation in the intact protein relative to the isolated regulatory domain, which is unrestricted in its conformational equilibrium between inactive and active states.

Linker Variations in OmpR/PhoB RRs. The linkers that connect the regulatory and effector domains in OmpR/PhoB RRs are highly variable with respect to both length and sequence. The exact boundaries of linkers are difficult to discern from sequence alignments in the absence of structural information. Linker lengths in OmpR/PhoB proteins of unknown structure have been estimated by comparing the number of residues between conserved landmark residues in the regulatory and effector domains to those from structurally characterized family members. Such analysis has indicated that linker lengths vary from ∼5 to 20 residues, with 90% of the linkers being <13 residues and ∼30% being only 5 residues in length (*9*). It has been previously proposed that the linker may be a conduit for communication between regulatory and effector domains (*56*). However, studies that examined the effects of variations in the length and sequence of the linker in OmpR indicated a significant degree of tolerance in linker composition (*57*). The results are consistent with the notion that the primary role of the linker is merely to tether the two domains.

The structure of inactive MtrA contains a linker of 9 residues, from Arg 121 to Arg 129, spanning 19.7 Å between the last residue of α5 of the regulatory domain and the first residue of β6 of the DNA-binding domain. It is possible that the length of this linker may be shorter when MtrA exists as an active dimer. The residue corresponding to Arg 122 is highly conserved in OmpR/PhoB family members (*24*). In eight different structures of active state regulatory domain dimers, this residue is found at the end of α5, participating in the dimer interface through the formation of an intermolecular salt bridge with the side chain of a conserved acidic residue (*21*, *23*−*25*). For the regulatory domain of MtrA to form an analogous dimer, Arg 122 would have to adopt a helical conformation, thus lengthening α5 and shortening the inter-domain linker. This suggests that the linker region within a given RR might vary as a function of activation state and that caution should be taken when attempting to categorize RRs based on linker lengths determined from sequence alignments.

There is now structural information for four different OmpR/PhoB family members with a range of linker lengths. DrrD and DrrB have relatively short linkers (4 and 5 residues, respectively), whereas MtrA and PrrA have longer linkers (9 residues for MtrA and 1 molecule of PrrA and 12 residues for the other molecule of PrrA). All four proteins have different arrangements of their regulatory and effector domains relative to each other (Figure 4). Not surprisingly, there is a correlation between the linker length and the domain orientations. RRs with orientations that position the C terminus of the regulatory domain in close proximity to the N terminus of the DNA-binding domain (DrrB and DrrD) have short linkers, whereas RRs with distant positioning of these residues (MtrA and PrrA) have longer linkers. Thus, linker length may have some predictive information with regard to domain orientation. About one-third of OmpR/PhoB family members have short linkers (*9*). These proteins must have domain orientations that position α5 of the regulatory domain near the β-platform of the DNA-binding domain. Longer linkers would not place this restriction on domain orientation. It should be noted, however, that linker length is not predictive of the nature of domain interfaces. DrrD, which lacks a domain interface, and DrrB, which has an extensive interface, contain linkers of similar lengths.

The 9-residue linker of MtrA is sufficient to reach almost half way around the DNA-binding domain. If the linker, that in all structures determined to date has few specific contacts with the DNA-binding domain, takes the shortest path between its points of attachment, then there are no orientations of the regulatory and DNA-binding domains that would require linkers of substantially greater length than that of MtrA. This perhaps explains why the distribution of linker lengths in OmpR/PhoB family members is biased toward shorter linkers (*9*). Perhaps the longer linkers, ranging up to ∼20 residues, take more convoluted paths around the DNA-binding domain, or adopt minor elements of secondary structure, such as the single helical turn of the linker that forms part of the domain interface in the RR methylesterase CheB (*58*). Such an arrangement would be distinctly different from those observed for the linkers of MtrA and PrrA that appear to be relatively flexible. These linkers lack specific packing interactions and appear to contribute little to the stabilization of the domain orientation in the inactive state,

thus providing no barrier to domain separation once the domain interface is disrupted by activation of the regulatory domain.

Domain Arrangements Confer Regulatory Strategies. The four crystal structures of inactive full-length OmpR/PhoB RRs determined to date all exhibit different orientations of their regulatory and effector domains. This is a distinct contrast to the many crystal structures of active OmpR/PhoB family regulatory domains that all display a similar dimer structure, consistent with a single common active state. The different inactive domain configurations appear to provide different mechanisms for regulating the transition between inactive and active states.

Our results suggest that the intramolecular interface in MtrA inhibits the DNA-binding activity of MtrA in three distinct ways: (1) it sterically blocks access to the recognition helix, (2) it blocks dimer formation by sequestering the α4-β5-α5 surface of the regulatory domain, and (3) it reduces the propensity for phosphorylation by trapping the regulatory domain in an inactive state. Thus, the domain configuration of inactive MtrA poses a substantial barrier to activation. This can be contrasted with the domain orientations in inactive *T. maritima* DrrD that expose the recognition helix and contain no domain interface (*31*), possibly posing a relatively low barrier to activation. These two extreme cases represent only a subset of many possible regulatory strategies that can be mediated by different domain arrangements in the inactive states of RRs. Additional regulatory strategies include the unique regulatory domain dimers observed for inactive *E. coli* PhoB (*21*, *30*) and *B. subtilis* PhoP (*34*), and the inhibitory interaction of the inactive regulatory domain of *E. coli* ArcA that blocks higher order oligomerization of the DNA-binding domain (*24*).

It seems likely that many of the previously documented differences in regulatory properties of different OmpR/PhoB family members such as the extent to which the regulatory domain plays inhibitory (*59*) versus activating roles (*57*, *60*) may be explained by variations in the domain arrangements in the inactive states. In the case of *M. tuberculosis* MtrA, the intramolecular domain interface of the inactive state may lead to a higher barrier to activation, allowing strict regulation of the transition between inactive and active states. Recent studies of *M. tuberculosis* growth in macrophages and mice lungs and spleens have indicated that an optimal ratio of phosphorylated to unphosphorylated MtrA is essential for bacterial proliferation (*45*). Thus, the configuration of domain interactions in the inactive state may be a critical feature of OmpR/PhoB RR design that allows the activation properties of each RR to be optimized for the specific regulatory needs of the two-component system in which it functions.

ACKNOWLEDGMENT

We thank Evan H. Bursey for assisting with X-ray data collection and Jayita Guhaniyogi for the synthesis of phosphoramidate.

REFERENCES

1. Hoch, J. A., and Silhavy, T. J., Eds. (1995) *Two-Component Signal Transduction*, pp 488, American Society for Microbiology Press, Washington, D.C.
2. Stock, A. M., Robinson, V. L., and Goudreau, P. N. (2000) Two-component signal transduction, *Annu. Rev. Biochem. 69*, 183−215.
3. Wadhams, G. H., and Armitage, J. P. (2004) Making sense of it all: bacterial chemotaxis, *Nat. Rev. Mol. Cell Biol. 5*, 1024−1037.
4. Beier, D., and Gross, R. (2006) Regulation of bacterial virulence by two-component systems, *Curr. Opin. Microbiol. 9*, 143−152.
5. Peterson, C. N., Mandel, M. J., and Silhavy, T. J. (2005) *Escherichia coli* starvation diets: essential nutrients weigh in distinctly, *J. Bacteriol. 187*, 7549−7553.
6. Miller, M. B., and Bassler, B. L. (2001) Quorum sensing in bacteria, *Annu. Rev. Microbiol. 55*, 165−199.
7. Stock, J. B., Ninfa, A. J., and Stock, A. M. (1989) Protein phosphorylation and regulation of adaptive responses in bacteria, *Microbiol. Rev. 53*, 450−490.
8. Galperin, M. Y. (2006) Structural classification of bacterial response regulators: diversity of output domains and domain combinations, *J. Bacteriol. 188*, 4169−4182.
9. Martinez-Hackert, E., and Stock, A. M. (1997) Structural relationships in the OmpR family of winged-helix transcription factors, *J. Mol. Biol. 269*, 301−312.
10. Igo, M. M., Ninfa, A. J., and Silhavy, T. J. (1989) A bacterial environmental sensor that functions as a protein kinase and stimulates transcriptional activation, *Genes Dev. 3*, 598−605.
11. Makino, K., Shinagawa, H., Amemura, M., Kawamoto, T., Yamada, M., and Nakata, A. (1989) Signal transduction in the phosphate regulon of *Escherichia coli* involves phosphotransfer between PhoR and PhoB proteins, *J. Mol. Biol. 210*, 551−559.
12. Fiedler, U., and Weiss, V. (1995) A common switch in activation of the response regulators NtrC and PhoB: phosphorylation induces dimerization of the receiver modules, *EMBO J. 14*, 3696−3705.
13. McCleary, W. R. (1996) The activation of PhoB by acetylphosphate, *Mol. Microbiol. 20*, 1155−1163.
14. Jeon, Y., Lee, Y. S., Han, J. S., Kim, J. B., and Hwang, D. S. (2001) Multimerization of phosphorylated and non-phosphorylated ArcA is necessary for the response regulator function of the Arc two-component signal transduction system, *J. Biol. Chem. 276*, 40873−40879.
15. Chen, Y., Birck, C., Samama, J. P., and Hulett, F. M. (2003) Residue R113 is essential for PhoP dimerization and function: a residue buried in the asymmetric PhoP dimer interface determined in the PhoPN three-dimensional crystal structure, *J. Bacteriol. 185*, 262−273.
16. Robinson, V. L., Wu, T., and Stock, A. M. (2003) Structural analysis of the domain interface in DrrB, a response regulator of the OmpR/PhoB subfamily, *J. Bacteriol. 185*, 4186−4194.
17. Birck, C., Mourey, L., Gouet, P., Fabry, B., Schumacher, J., Rousseau, P., Kahn, D., and Samama, J.-P. (1999) Conformational changes induced by phosphorylation of the FixJ receiver domain, *Struct. Fold. Des. 7*, 1505−1515.
18. Kern, D., Volkman, B. F., Luginbuhl, P., Nohaile, M. J., Kustu, S., and Wemmer, D. E. (1999) Structure of a transiently phosphorylated switch in bacterial signal transduction, *Nature 40*, 894−898.
19. Lewis, R. J., Brannigan, J. A., Muchová, K., Barák, I., and Wilkinson, A. J. (1999) Phosphorylated aspartate in the structure of a response regulator protein, *J. Mol. Biol. 294*, 9−15.
20. Halkides, C. J., McEvoy, M. M., Casper, E., Matsumura, P., Volz, K., and Dahlquist, F. W. (2000) The 1.9 Å resolution crystal structure of phosphono-CheY, an analogue of the active form of the response regulator, CheY, *Biochemistry 39*, 5280−5286.
21. Bachhawat, P., Swapna, G. V., Montelione, G. T., and Stock, A. M. (2005) Mechanism of activation for transcription factor PhoB suggested by different modes of dimerization in the inactive and active states, *Structure 13*, 1353−1363.
22. Volkman, B. F., Lipson, D., Wemmer, D. E., and Kern, D. (2001) Two-state allosteric behavior in a single domain signaling protein, *Science 291*, 2429−2433.
23. Bent, C. J., Isaacs, N. W., Mitchell, T. J., and Riboldi-Tunnicliffe, A. (2004) Crystal structure of the response regulator 02 receiver domain, the essential YycF two-component system of *Streptococcus pneumoniae* in both complexed and native states, *J. Bacteriol. 186*, 2872−2879.
24. Toro-Roman, A., Mack, T. R., and Stock, A. M. (2005) Structural analysis and solution studies of the activated regulatory domain of the response regulator ArcA: a symmetric dimer mediated by the α4-β5-α5 face, *J. Mol. Biol. 349*, 11−26.
25. Toro-Roman, A., Wu, T., and Stock, A. M. (2005) A common dimerization interface in bacterial response regulators KdpE and TorR, *Protein Sci. 14*, 3077−3388.

26. Makino, K., Shinagawa, H., Amemura, M., and Nakata, A. (1986) Nucleotide sequence of the *phoB* gene, the positive regulatory gene for the phosphate regulon of *Escherichia coli* K-12, *J. Mol. Biol. 190*, 37−44.
27. Pratt, L. A., and Silhavy, T. J. (1995) Identification of base pairs important for OmpR-DNA interaction, *Mol. Microbiol. 17*, 565−573.
28. Simon, G., Jourlin, C., Ansaldi, M., Pascal, M. C., Chippaux, M., and Mejean, V. (1995) Binding of the TorR regulator to cis-acting direct repeats activates *tor* operon expression, *Mol. Microbiol. 17*, 971−980.
29. Lynch, A. S., and Lin, E. C. (1996) Transcriptional control mediated by the ArcA two-component response regultor protein of *Escherichia coli*: characterization of DNA binding at target promoters, *J. Bacteriol. 178*, 6238−6249.
30. Blanco, A. G., Sola, M., Gomis-Ruth, F. X., and Coll, M. (2002) Tandem DNA recognition by PhoB, a two-component signal transduction transcriptional activator, *Structure 10*, 701−713.
31. Buckler, D. R., Zhou, Y., and Stock, A. M. (2002) Evidence of intradomain and interdomain flexibility in an OmpR/PhoB homolog from, *Thermotoga maritima*, *Structure 10*, 153−164.
32. Nowak, E., Panjikar, S., Konarev, P., Svergun, D. I., and Tucker, P. A. (2006) The structural basis of signal transduction for the response regulator PrrA from *Mycobacterium tuberculosis*, *J. Biol. Chem. 281*, 9659−9666.
33. Solà, M., Gomis-Rüth, F. X., Serrano, L., González, A., and Coll, M. (1999) Three-dimensional crystal structure of the transcription factor PhoB receiver domain, *J. Mol. Biol. 285*, 675−687.
34. Birck, C., Chen, Y., Hulett, F. M., and Samama, J. P. (2003) The crystal structure of the phosphorylation domain in PhoP reveals a functional tandem association mediated by an asymmetric interface, *J. Bacteriol. 185*, 254−261.
35. Via, L. E., Curcic, R., Mudd, M. H., Dhandayuthapani, S., Ulmer, R. J., and Deretic, V. (1996) Elements of signal transduction in *Mycobacterium tuberculosis*: *in vitro* phosphorylation and *in vivo* expression of the response regulator MtrA, *J. Bacteriol. 178*, 3314−3321.
36. Zahrt, T. C., and Deretic, V. (2000) An essential two-component signal transduction system in *Mycobacterium tuberculosis*, *J. Bacteriol. 182*, 3832−3838.
37. Sheridan, R. C., McCullough, J. F., and Wakefield, Z. T. (1971) Phosphoramidic acid and its salts, *Inorg. Synth. 13*, 23−26.
38. Buckler, D. R., and Stock, A. M. (2000) Synthesis of [^{32}P]-phosphoramidate for use as a low molecular weight phosphodonor reagent, *Anal. Biochem. 283*, 222−227.
39. Waldo, G. S., Standish, B. M., Berendzen, J., and Terwilliger, T. C. (1999) Rapid protein-folding assay using green fluorescent protein, *Nat. Biotechnol. 17*, 691−695.
40. Otwinowski, Z., and Minor, W. (1997) Processing of X-ray diffraction data collected in oscillation mode, *Methods Enzymol. 276*, 307−326.
41. Bricogne, G., Vonrhein, C., Flensburg, C., Schiltz, M., and Paciorek, W. (2003) Generation, representation and flow of phase information in structure determination: recent developments in and around SHARP 2.0, *Acta Crystallogr., Sect. D 59*, 2023−2030.
42. Morris, R. J., Perrakis, A., and Lamzin, V. S. (2003) ARP/wARP and automatic interpretation of protein electron density maps, *Methods Enzymol. 374*, 229−244.
43. Emsley, P., and Cowtan, K. (2004) Coot: model-building tools for molecular graphics, *Acta Crystallogr., Sect. D 60*, 2126−2132.
44. Adams, P. D., Gopal, K., Grosse-Kunstleve, R. W., Hung, L. W., Ioerger, T. R., McCoy, A. J., Moriarty, N. W., Pai, R. K., Read, R. J., Romo, T. D., Sacchettini, J. C., Sauter, N. K., Storoni, L. C., and Terwilliger, T. C. (2004) Recent developments in the PHENIX software for automated crystallographic structure determination, *J. Synchrotron Radiat. 11*, 53−55.
45. Fol, M., Chauhan, A., Nair, N. K., Maloney, E., Moomey, M., Jagannath, C., Madiraju, M. V., and Rajagopalan, M. (2006) Modulation of *Mycobacterium tuberculosis* proliferation by MtrA, an essential two-component response regulator, *Mol. Microbiol. 60*, 643−657.
46. Kraulis, P. J. (1991) MOLSCRIPT: A program to produce both detailed and schematic plots of protein structures, *J. Appl. Crystallogr. 24*, 946−950.
47. Merritt, E. A., and Bacon, D. J. (1997) Raster3D: photorealistic molecular graphics, *Methods Enzymol. 277*, 505−524.
48. Stock, A. M., Martinez-Hackert, E., Rasmussen, B. F., West, A. H., Stock, J. B., Ringe, D., and Petsko, G. A. (1993) Structure of the Mg^{2+}-bound form of CheY and mechanism of phosphoryl transfer in bacterial chemotaxis, *Biochemistry 32*, 13375−13380.
49. Harding, M. M. (2006) Small revisions to predicted distances around metal sites in proteins, *Acta Crystallogr., Sect. D 62*, 678−682.
50. Pratt, L. A., and Silhavy, T. J. (1994) OmpR mutants specifically defective for transcriptional activation, *J. Mol. Biol. 243*, 579−594.
51. Lukat, G. S., McCleary, W. R., Stock, A. M., and Stock, J. B. (1992) Phosphorylation of bacterial response regulator proteins by low molecular weight phospho-donors, *Proc. Natl. Acad. Sci. U.S.A. 89*, 718−722.
52. Eisenmesser, E. Z., Millet, O., Labeikovsky, W., Korzhnev, D. M., Wolf-Watz, M., Bosco, D. A., Skalicky, J. J., Kay, L. E., and Kern, D. (2005) Intrinsic dynamics of an enzyme underlies catalysis, *Nature 438*, 117−121.
53. Da Re, S., Schumacher, J., Rousseau, P., Fourment, J., Ebel, C., and Kahn, D. (1999) Phosphorylation-induced dimerization of the FixJ receiver domain, *Mol. Microbiol. 34*, 504−511.
54. Ames, S. K., Frankema, N., and Kenney, L. J. (1999) C-terminal DNA binding stimulates N-terminal phosphorylation of the outer membrane protein regulator OmpR from *Escherichia coli*, *Proc. Natl. Acad. Sci. U.S.A. 96*, 11792−11797.
55. Schuster, M., Silversmith, R. E., and Bourret, R. B. (2001) Conformational coupling in the chemotaxis response regulator CheY, *Proc. Natl. Acad. Sci. U.S.A. 98*, 6003−6008.
56. Mattison, K., Oropeza, R., and Kenney, L. J. (2002) The linker region plays an important role in the inter-domain communication of the response regulator OmpR, *J. Biol. Chem. 277*, 32714−32721.
57. Walthers, D., Tran, V. K., and Kenney, L. J. (2003) Interdomain linkers of homologous response regulators determine their mechanism of action, *J. Bacteriol. 185*, 317−324.
58. Djordjevic, S., Goudreau, P. N., Xu, Q., Stock, A. M., and West, A. H. (1998) Structural basis for methylesterase CheB regulation by a phosphorylation-activated domain, *Proc. Natl. Acad. Sci. U.S.A. 95*, 1381−1386.
59. Ellison, D. W., and McCleary, W. R. (2000) The unphosphorylated receiver domain of PhoB silences the activity of its output domain, *J. Bacteriol. 182*, 6592−6597.
60. Tsuzuki, M., Aiba, H., and Mizuno, T. (1994) Gene activation by the *Escherichia coli* positive regulator, OmpR: phosphorylation-independent mechanism of activation by an OmpR mutant, *J. Mol. Biol. 242*, 607−613.

BI602546Q